Applications of Magnetic Resonance Microscopy

ROBERT R. MARONPOT,[1] ROBERT C. SILLS,[1] AND G. ALLAN JOHNSON[2]

[1]*National Institute of Environmental Health Sciences, Research Triangle Park, North Carolina 27709, USA and*
[2]*Duke Center for In Vivo Microscopy, Duke University Medical Center, Durham, North Carolina 27710, USA*

ABSTRACT

Magnetic resonance imaging (MRI) has enjoyed enormous clinical success since the first demonstration of the method more than 30 years ago. An increasing number of pharmaceutical manufacturers seeking new biomarkers for assessing drug efficacy and toxicity are turning to MRI. A specific application of MRI promises to revolutionize pathology for the basic scientist in the same way MRI has forever altered the standard of care in the clinical domain. More specifically, this application is the use of magnetic resonance microscopy (MRM) in conjunction with new staining methodologies that now make MRM routinely available to the widest range of investigators.

Keywords. Mouse; imaging; phenotype; MRI; rat; carbonyl sulfide.

HOW DOES MRM WORK?

Magnetic resonance microscopy (MRM)[1] is based on the same physical principles as its clinical cousin, MRI. Unpaired protons placed in a strong magnetic field precess at a very explicit frequency. These protons interact with an applied oscillating magnetic field at the same (resonant) frequency, absorbing and re-emitting energy in ways that can be spatially encoded to generate a digital image. Several excellent reviews (Haacke et al., 1999) offer complete descriptions of nuclear magnetic resonance (NMR) and spatial encoding.

The fathers of MRI realized the potential for encoding at microscopic resolution (Lauterbur, 1973; Mansfield and Grannell, 1975). This realization was reduced to practice by 2 groups in 1986 (Eccles and Callaghan, 1986; Johnson et al., 1986). Figure 1 shows the difference between MRI and MRM. The images are digital image arrays in which each discrete image element (pixel) represents the signal from a small tissue volume (voxel). In the clinical image in Figure 1a, each pixel represents the signal from a voxel in a 5-mm slice. The spatial resolution in the coronal plane pictured is 1×1 mm, i.e., each voxel is 5 mm^3. By comparison, the pixels in the mouse brain in Figure 1b represent the signal from a voxel that is $40 \times 40 \times 40$ microns, i.e., a volume nearly 80,000 times smaller than that of the clinical image.

Achieving this spatial resolution has been the technical focus of a number of laboratories over the last 25 years. The first barrier involves the gradient coils used for spatial encoding. Spatial encoding is achieved in MRI and MRM through the use of magnetic field gradients. The protons of the specimen all resonate at the Larmor frequency for the field in which the protons are immersed. At 1.5 Tesla, the operational field for a clinical scanner, the protons resonate at 64 MHz. The gradi-

ents act to alter the magnetic field along the direction they are applied. A gradient along the z axis causes the field to vary along that axis. Application of a narrow radio frequency pulse at 64 MHz in the presence of this strong gradient excites only those protons in a very narrow slice, which satisfies the resonance condition. Thus, to make higher resolution images, one must use much stronger gradients. The gradients for MRM are typically 50–100 times those of clinical systems.

Sensitivity is the second major barrier. Since the voxels for MRM can be 100,000 times smaller than those in MRI, the signal will be 100,000 times weaker. A number of approaches are used to generate sufficient sensitivity for MRM. MRM is typically done at higher magnetic fields where the signal is stronger. Radio frequency coils, i.e., the antennae used to capture the weak radio frequency signal, are carefully designed to ensure the highest sensitivity (Hurlston et al., 1997). Specialized encoding strategies have been devised to optimize efficiency (Suddarth and Johnson, 1991). Using these collective strategies, we have acquired images with excellent signal to noise at spatial resolution down to $20 \times 20 \times 20$ microns (8×10^{-6} mm^3)—over a million times higher resolution than is typical for a clinical body scan (Johnson et al., 2002a).

The use of MRM in histology was first suggested in 1993 (Johnson et al., 1993). Motion, a major limitation to the spatial resolution in live animal studies, does not pose a barrier for fixed tissues. With the initial applications in fixed specimens, the enormous potential became clear for novel methods to fix and stain tissue for MRM. The concept of active stains was more recently introduced in which fixatives and fixation methods have been developed with an explicit goal of very high resolution 3-dimensional imaging (Johnson et al., 2002b). This development of active stains is now making MRM possible on a routine basis.

Advantages, Strengths, and Weaknesses of MRM

Just as MRI did not replace computed tomography (CT) in the clinical arena, MRM will not replace more traditional optical methods. Instead, MRM will complement existing methods. Four fundamental factors distinguish MRM from existing optical histology:
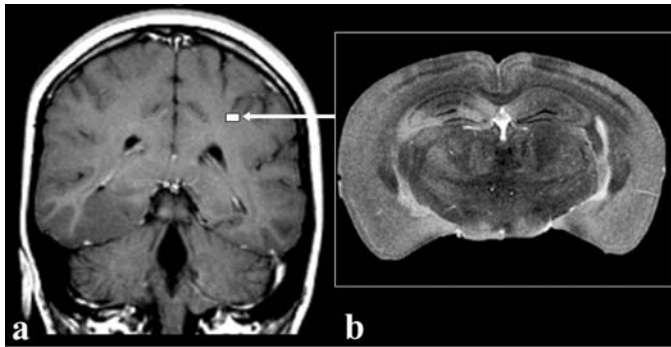

FIGURE 1.—Comparison of (a) a clinical MRI showing a 5-mm slice of human brain compared to (b) a 40-micron MRM slice of mouse brain. The size of the mouse brain relative to the human brain is depicted by the white square (arrow). The voxels in the mouse brain image represents a volume 80,000 times smaller than the voxels in the clinical image.

- MRM is nondestructive
- MRM takes advantage of unique "proton" stains
- MRM is inherently 3-dimensional
- MRM is inherently digital.

The "slice" in an MRM image is produced "electronically," i.e., through the simultaneous interaction of the radio frequency pulses and the spatial encoding gradients. Thus, the specimen is *not* physically sectioned. Figure 2 shows a comparison between a wild-type mouse (Figure 2a and 2c) and a mouse in which the uricase enzyme has been knocked out (Figure 2b and 2d) (Kelly et al., 2001). The specimen remains intact, which offers these advantages:

- The specimen can be sliced along the transverse plane (Figure 2a and 2b) or the coronal plane (Figure 2c and 2d).
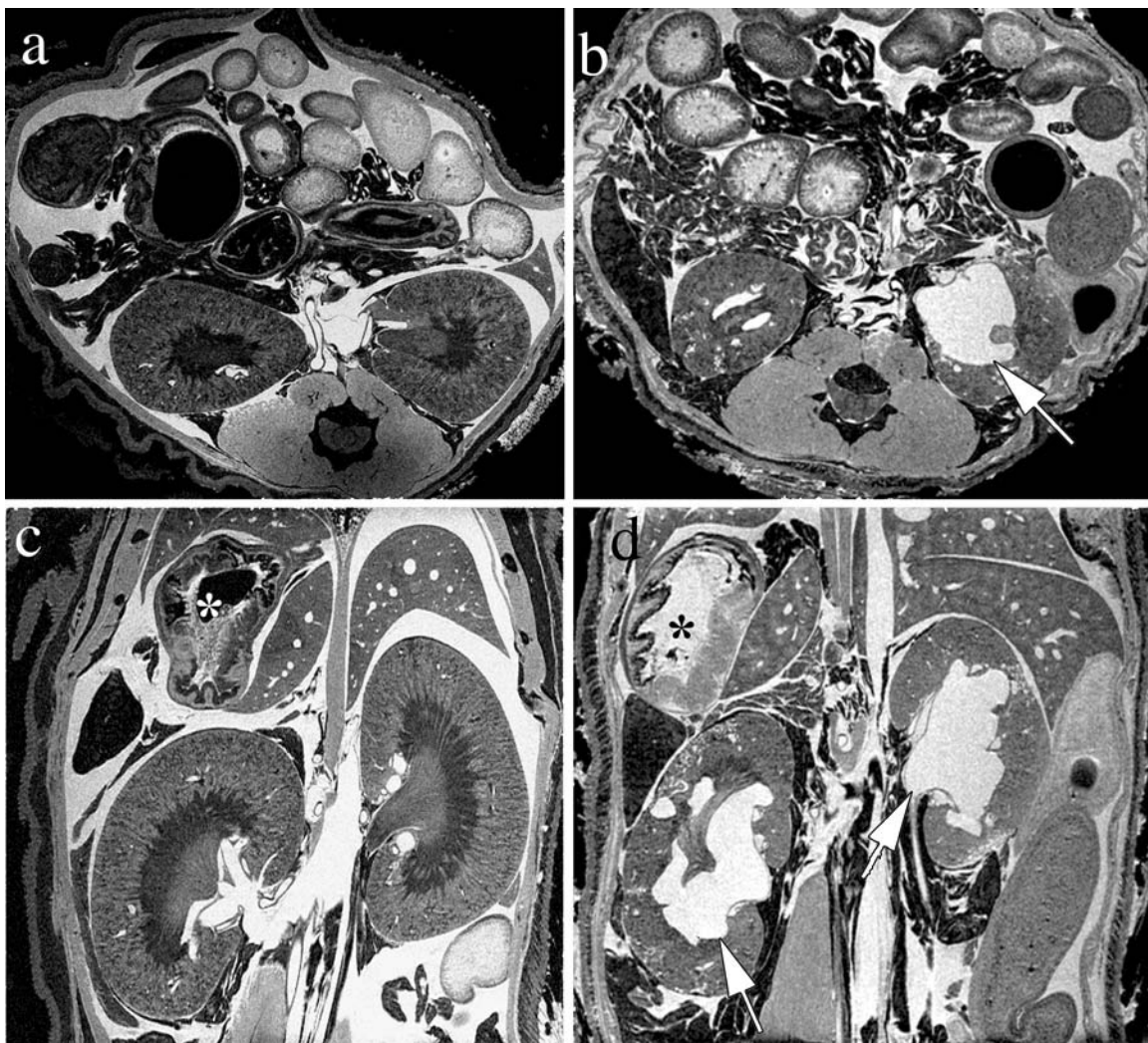

FIGURE 2.—Comparison of (a and c) wild-type and (b and d) uricase KO mice shown in axial (a and b) and coronal (c and d) planes. These 50-micron slices clearly show multiple renal cysts and the dilated renal pelvis (arrows) in the uricase KO mouse. The resolution is sufficient to clearly show the distinction between renal cortex and medulla in the wild-type mouse as well as the glandular and nonglandular stomach mucosa (asterisks).

- The specimen can be scanned in many different ways, at different resolutions, through different planes. The coronal slices shown in Figure 2c and 2d are from the same volume set as shown in Figures 2a and 2b, viewed along the orthogonal plane.
- The 2 slices can be carefully matched to compare the anatomy. Since no distortion occurs from dehydration and physical sectioning, morphometric measurements are much more accurate than could ever be made with traditional glass slides.

We use the term "proton stain" to refer to the contrast in the image. For example in clinical CT, the contrast is determined by the X-ray density of the tissue. Bone (very dense), is white, while the lung (mostly air), is dark. The superb soft tissue contrast that distinguishes MRI from CT arises from the proton content in the tissue and the physical/chemical properties of the protons. Protons in fat yield different MR signals than protons in muscle. Note for example in Figure 2c, the distinction between kidney cortex and medulla, the layers of the gastric mucosa, and the differences between the muscle and fat.

Much of the success of MRI comes from its superb sensitivity to pathologic alterations. Tumors, inflammation, and cellular proliferation are all evident because of the changes that are induced in the tissue water and how the protons are bound in the tissue. Figures 3 and 4 show excellent examples from a recent toxicology study of carbonyl sulfide. Malacic lesions in the parietal cortex (Figure 3a, c, d) are seen as bright areas

where there has been substantial alteration of the blood–brain barrier. The brain has been actively stained with a mixture of formalin and gadolinium-diethylenetriaminepentaacetic acid (Gd-DTPA) (Johnson et al., 2002b). The Gd has unpaired electrons that alter the signal from the tissue. In the areas of the cortical lesion, significant breakdown in the blood–brain barrier results in an increased concentration of the formalin mixture. Inflammatory lesions in the posterior colliculus (Figure 3b, d) are seen as a dark region arising from necrosis.

Figure 4 demonstrates a comparison between MRM and optical hematoxylin and eosin (H&E) sections from the same study. Bilaterally symmetrical hypointense regions representing necrosis are again evident in this case involving the zona inserta of the hypothalamus. These MRM lesions correlate with malacia and inflammation in the corresponding optical sections.

The unique 3-dimensional nature of MRM is also demonstrated in Figure 3. The individual electronic slices (Figure 3a and 3b) are each part of a 3-dimensional array. Three-dimensional, volume imaging software (Vitrea 2.0, Vital Images, Inc., Minneapolis MN) allows us to mark the lesions in the 2-dimensional slices and then render the entire volume. In Figure 3c, the rendered volume shows a reflected image that outlines the surface features. Note how the cortical lesion can be easily related to the surface vessels, giving some hint to the mechanism that gives rise to the lesion. The same software allows interactive changes to the rendering parameters. Since each element of the volume image has a
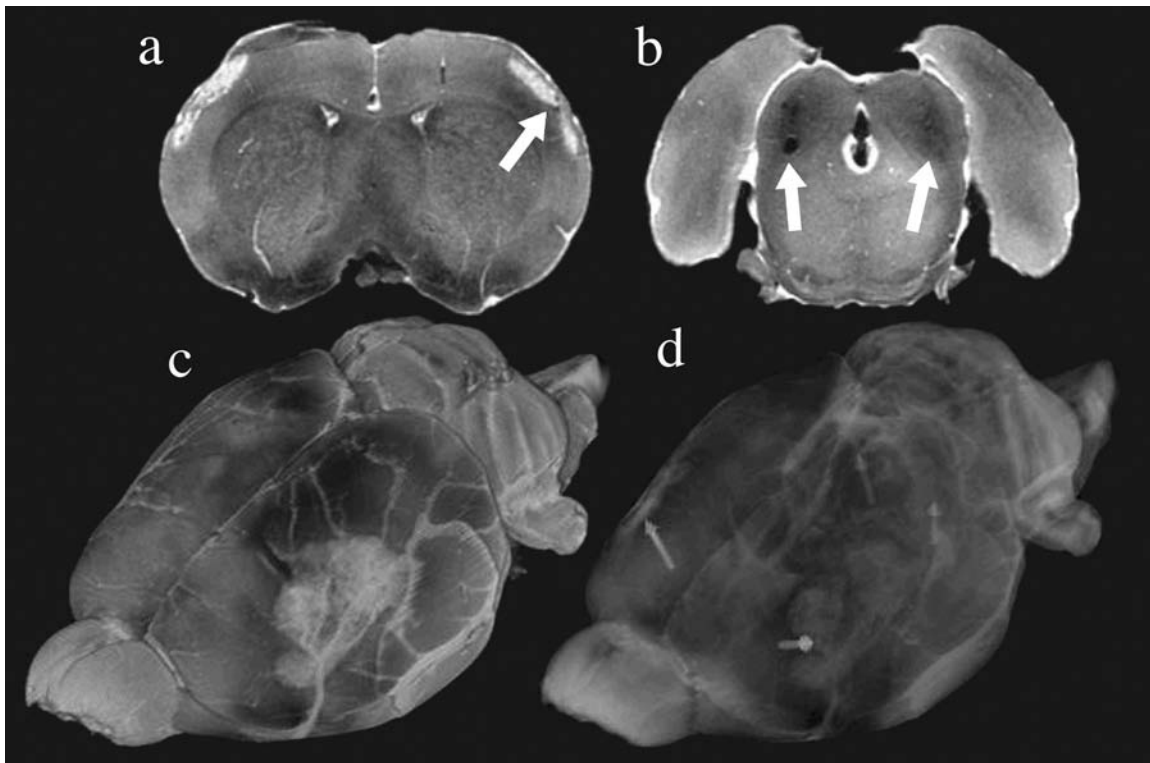

FIGURE 3.—Axial (a and b) and volume rendered (c and d) MRM images of the brain from a male F344 rat exposed to 600 ppm carbonyl sulfide for 2 days. Malacic lesions (a) are present in the parietal cortex (single large white arrow) and the volume of the lesion can be appreciated in the volume rendered image (c and d—gray arrows). Inflammatory and necrotic lesions in the posterior colliculus (b—double large white arrows) yield a dark MRM signal.
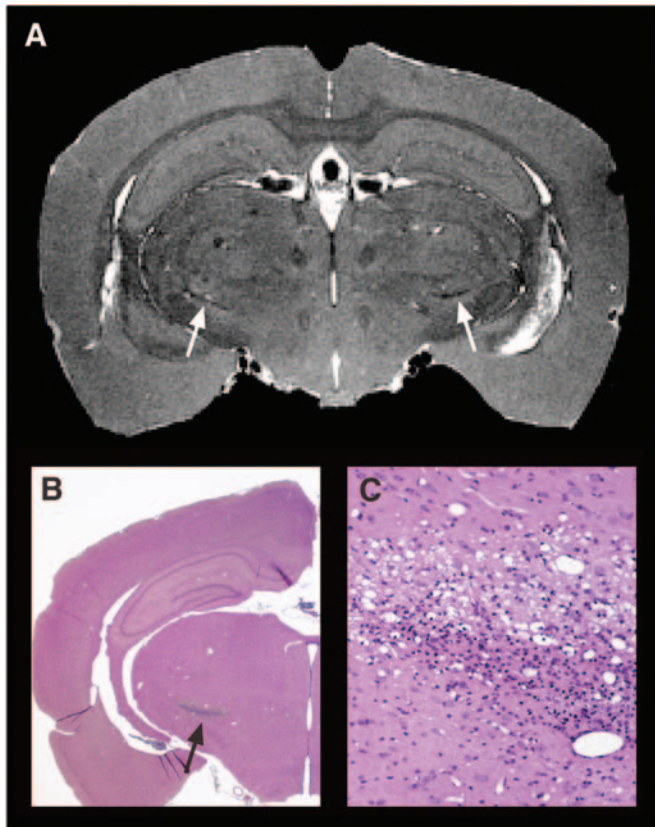
FIGURE 4.—Male F344 rats exposed to 600 ppm carbonyl sulfide for 2 days (6 hours/day) and sacrificed at 2 weeks. Transverse slice through the brain (70 microns) at 9.4 T. (A) Note the bilateral symmetrical hypointense areas in the hypothalamus (arrows); (B) In matching hematoxylin and eosin (H&E) stained section, note the excellent correlation between the MRM image and the light microscopic image (2.5×); (C) The hypointense areas in the zona inserta of the hypothalamus in (A) localize to focal accumulations of microglial cells in a prior area of necrosis (×20).

unique location and signal intensity, one can adjust the parameters that are used to make selected tissues transparent. This has been done in Figure 3d to allow simultaneous rendering of the tissue surface and the points within the volume that have been marked on the 2-dimensional slices (Figure 3a and 3b). This information provides valuable guidance in choosing the locations from which H&E sections can be made. One can, in effect, survey the whole brain electronically, mark areas of interest, interactively display the volume, and choose the levels at which optical sections are then made.

MR microscopy images are inherently digital, which has enormous practical implications. Figure 5 shows a comparison of an MRM image of an 18-day rat fetus in a teratology study. The whole 2-mm razor blade tissue slice in Figure 5a demonstrates the anatomy of the thoracic cavity, chambers of the heart, spinal cord, and lung in this Bouin's fixed fetus—but so does the comparable digital MR image shown in Figure 5b. The single level in Figure 5b is one of 512 transverse sections. With a simple command, one can view the same anatomy from a different perspective as shown in Figure 5c. Since these sections are all digital, one can move

back and forth to adjacent slices by a simple stroke of an interactive slider. One can choose alternative planes, use digital magnification, alter contrast and brightness, and perform digital measurements. A survey of the entire fetus can be accomplished quickly. Moreover, the digital record is permanent. Lesions, anatomical anomalies, or areas of concern can be marked. Images can be incorporated into reports with a click of the mouse. And the entire 3-dimensional array can be stored in a digital archive that can be searched for similar findings. Finally, the fixed specimen can be submitted for conventional optical microscopy.

Currently, MRM has 2 major weaknesses. The first weakness is the newness of the method. Since the contrast is dependent on mechanisms that are entirely different from those pathologists have seen previously, the interpretation of normal anatomy and pathology must be learned. Seeing an MR histology image is much like seeing an H&E slide for the first time. There is a learning curve for the skills that must be mastered. The second weakness is the accessibility of the technique. The equipment required is expensive. More importantly, the technical personnel required to develop and support the technology are in very short supply. Establishing the capability to perform MRM at a new site requires a bare minimum of $3 million in capital equipment, at least 4 people with very sophisticated training, and a minimum of 18 months for setup.

MRM Compliments Optical Microscopy

Magnetic resonance microscopy is an entirely new approach to pathology. It will not replace conventional optical sections. MRM will complement more traditional methods. and can yield enormous gains in efficiency with consequent reductions in cost. The images in Figure 3 were generated and delivered to the desktop for examination in less than 24 hours. The staining method is a straightforward extension of conventional perfusion fixation. Tissues were not dehydrated, so the images could be generated as soon as the tissue was fixed. The scan time was <4 hours and resulted in 256 slices covering the entire brain. Review of the slices to locate areas of interest took less than 5 minutes. The staining method is consistent with more traditional staining so once the areas of interest are identified, H&E sections are easily recovered. At $10–$15 per slice, sectioning the entire brain with a conventional microtome as shown in Figure 3 would be prohibitive ($4,000).

The two $(512)^3$ image arrays compared in Figure 2 would conservatively cost more than $7,500 each using conventional microtomy. Review of so many glass slides would be even more time-consuming with pathologists who are frequently already overloaded. This rapid digital review takes so little time that substantial cost savings are realized simply in the costs of interpretation. The digital records also provide an online archive. Storage costs for these online archives are trivial compared to the cost of glass slide archives. And, the efficiency of the entire process, the ability to distribute to multiple sites, and the true volumetric quantitative measurement capability will certainly have significant cost benefits.

MRM will also be a complement to in vivo studies. Where longitudinal studies are warranted, in vivo studies with MRI provide exciting new options. But the resolution in these
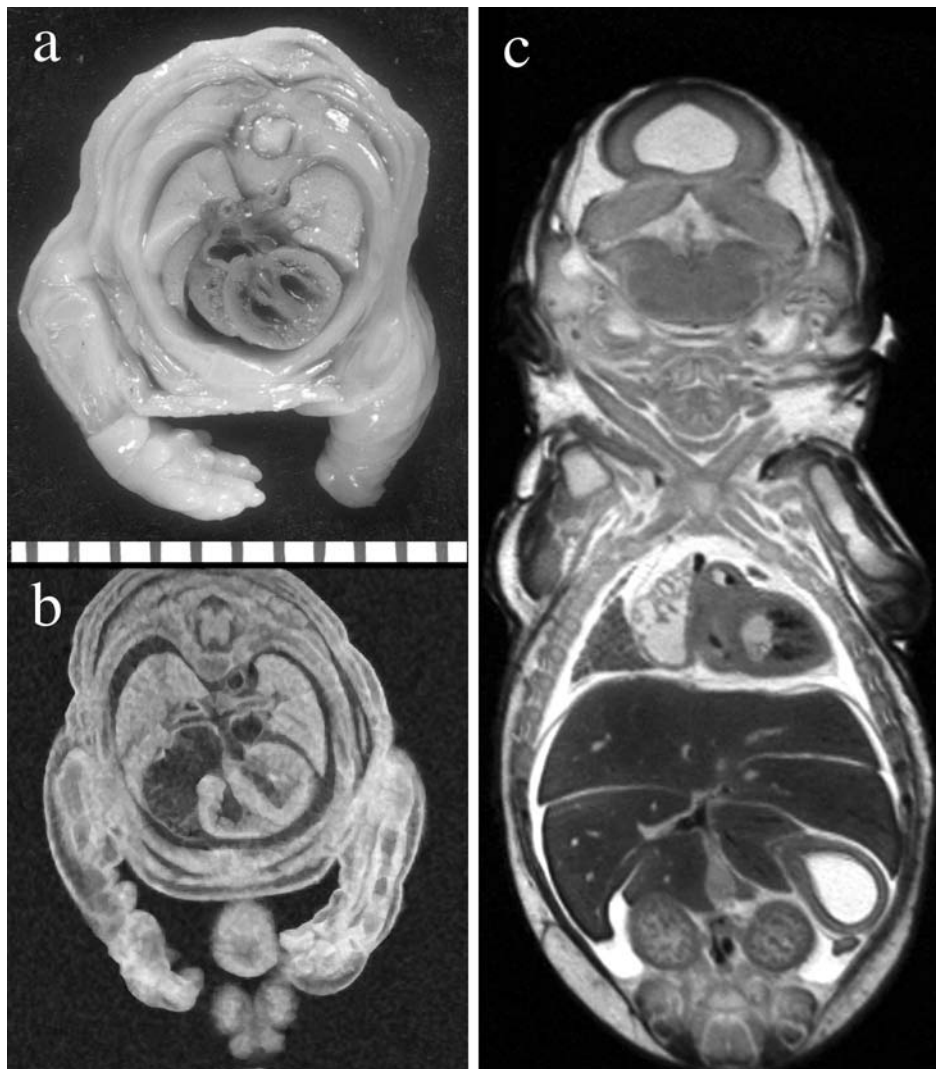
FIGURE 5.—An 18-day-old F344 rat fetus from a teratology study. A 2-mm razor blade slice through the thoracic cavity in a Bouin's fixed normal fetus (a) can be compared to a 100-micron electronic MRM slice (b). A coronal view (c) shows the anatomic detail from a different perspective. Vertical ruler marks are 1 mm apart.

in vivo studies will not approach that of fixed tissue MRM exams. Cardiac and respiratory motion and the complexities of life support will continue to keep the costs of in vivo studies much higher than the MRM studies on fixed specimens. But where in vivo studies are warranted, there will be substantial value for MRM studies on fixed specimens at the end point of the study to provide a more definitive image than can be obtained in the live animal.

Partnerships

MRM has been developed by the Duke University Center for In Vivo Microscopy under the direct sponsorship of the NIH-National Center for Research Resources and the National Cancer Institute. The Duke center has pioneered the development of this technology for more than 20 years. To date, MRM has been experimental—"bleeding edge." Demonstration of the utility and translation to real-world applications has been the goal of collaboration with scientists at the National Institute of Environmental Health Sciences (NIEHS),

Research Triangle Park, NC. What has been a partnership between government and academia is taking on commercial life with the formation of MRPath, Inc., a startup venture designed to translate MRM to the broadest possible community. Technical developments continue at the Duke Center for In Vivo Microscopy. Application of the technology to the challenging issues in toxicology, teratology, and morphologic phenotyping is now under way with investigators at NIEHS. MRPath has engaged a multidisciplinary team of pathologists, engineers, histology technicians, and computer scientists to take the technology from the laboratory to the desktop.

Figure 6 demonstrates the first fruits of the partnership between Duke, NIEHS, and MRPath. Figure 6a is a single coronal slice from a $512 \times 512 \times 1920$ three-dimensional image array that covers an entire mouse. "The Visible Mouse Project" (Johnson et al., 2002b) is an effort to develop an online, 3-dimensional atlas of the C57BL/6J mouse with complete anatomic annotation. As with most clinical imaging methods, development of the imaging approach has
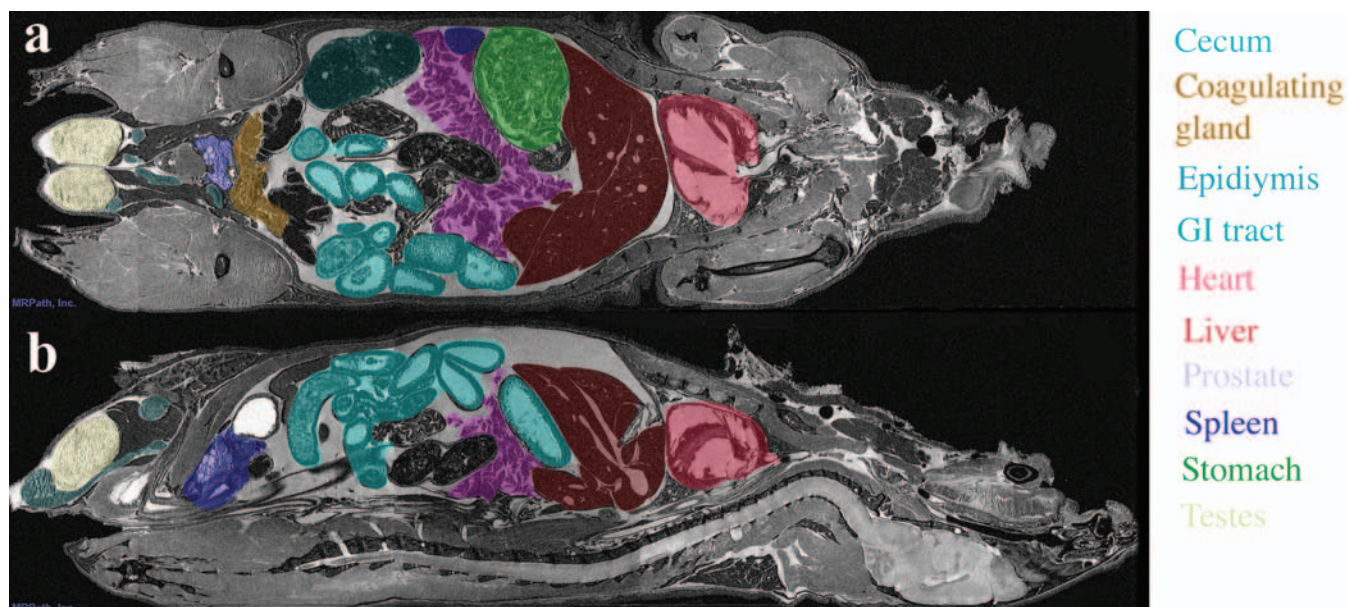
FIGURE 6.—A single coronal (a) and sagittal (b) slice taken from a 512 × 512 × 1920 three-dimensional image array of an entire 25-gram C57BL/6 mouse. Image resolution is 50 × 50 × 50 microns in the x, y, and z planes. Organs have been traced and color-coded for identification.

preceded the application. The pathologist is presented the daunting task of interpreting "normal" anatomy with this new imaging modality, with little information about the sophisticated basis of contrast underlying the method. The "Visible Mouse" will help all the interested parties in the learning curve for magnetic resonance (MR) histology. The mouse in this image has been actively stained and scanned at 7.0 T at an unprecedented spatial resolution of 50 × 50 × 50 microns.

Critical organs and anatomical landmarks have been carefully identified. A flexible, general purpose image display program (Image J available at ⟨http://rsb.info.nih.gov/ij/⟩) has been modified to accommodate the dataset and labels. The user seeking to learn the MR anatomy of the mouse can turn on specific organs and anatomic landmarks from a list of more than 50. The landmarks have been color-coded so they overlay the underlying grayscale image. One can highlight all the organs of a system such as the digestive track, or find complex 3-dimensional relations between organs, for example, the liver, pancreas, and spleen. The isotropic nature of the data allows visualization in any plane, for example, the sagittal plane shown in Figure 6b.

CONCLUSION

What has been a laboratory curiosity dominated by technical development has matured to the point of biological application. Toxicologic pathology now has a new tool in its armamentarium that will permit an important adjunct to conventional optical microscopy, thus allowing for a more comprehensive evaluation of fixed specimens and perfusion fixed whole animals. In parallel, advances continue in the area of live animal imaging with the potential for studies that will allow longitudinal demonstration of tissue changes in animals. Magnetic resonance microscopy promises to revolutionize the fields of pathology, toxicology, and molecular biology by providing Web-deliverable 3D-microscopic images of specimens ranging from the embryo to the whole mouse or rat.

REFERENCES

Eccles, C. D., and Callaghan, P. T. (1986). High resolution imaging: the NMR microscope. *J Magn Reson* **68**, 393–8.

Haacke, E. M., Brown, R. W., Thompson, M. R., and Venkatesan, R. (1999). *Magnetic Resonance Imaging: Physical Principles and Sequence Design*. Wiley-Liss, New York.

Hurlston, S. E., Cofer, G. P., and Johnson, G. A. (1997). Optimized receiver coils for increased SNR in MR Microscopy. *Intl J Imaging Syst Technol* **8**, 277–84.

Johnson, G. A., Benveniste, H., Black, R. D., Hedlund, L. W., Maronpot, R. R., and Smith, B. R. (1993). Histology by magnetic resonance microscopy. *Magn Reson Quar* **9**, 1–30.

Johnson, G. A., Cofer, G. P., Fubara, B., Gewalt, S. L., Hedlund, L. W., and Maronpot, R. R. (2002a). Magnetic resonance histology for structural phenotyping. *J Mag Reson Imag* **16**, 423–9.

Johnson, G. A., Cofer, G. P., Gewalt, S. L., and Hedlund, L. W. (2002b). Morphologic phenotyping with magnetic resonance microscopy: the visible mouse. *Radiology* **222**, 789–93.

Johnson, G. A., Thompson, M. B., Gewalt, S. L., and Hayes, C. E. (1986). Nuclear magnetic resonance imaging at microscopic resolution. *J Magn Reson* **68**, 129–37.

Kelly, S. J., Delnomdedieu, M., Oliverio, M. I., Williams, L. D., Saifer, M. G. P., Sherman, M. R., Coffman, T. M., Johnson, G. A., and Hershfield, M. S. (2001). Diabetes insipidus in uricase-deficient mice: a model for evaluating therapy with poly(ethylene glycol)-uricase. *J Am Soc Nephrol* **12**, 1001–9.

Lauterbur, P. C. (1973). Image formation by induced local interactions—examples employing nuclear magnetic resonance. *Nature* **242**, 190–1.

Mansfield, P., and Grannell, P. K. (1975). Diffraction in microscopy in solids and liquids by NMR. *Phys Rev B* **12**, 3618.

Suddarth, S. A., and Johnson, G. A. (1991). Three-dimensional MR microscopy with large arrays. *Magn Reson Med* **18**, 132–41.